Poultry Science®

Gene coexpression network analysis reveals the genes and pathways in pectoralis major muscle and liver associated with wooden breast in broilers

Jun Lu,[1,*] Hui Yuan ,[1,2,*] Shengnan Liu,[*] Yuan Liu,[*] Ziwen Qin,[*] Wenpeng Han,[†] and Runxiang Zhang [*]

[*]*College of Animal Science and Technology, Northeast Agricultural University, Harbin 150030, Heilongjiang, China; and* [†]*Department of Biotechnology, Jieyang Polytechnic, Jieyang City 522000, Guangdong Province, China*

ABSTRACT Wooden breast (**WB**) is a myopathy mainly affecting pectoralis major (**PM**) muscle in modern commercial broiler chickens, causing enormous economic losses in the poultry industry. Recent studies have observed hepatic and PM muscle injury in broilers affected by WB, but the relationships between WB and the 2 tissues are mostly unclear. In the current study, the RNA-seq raw data of PM muscle and liver were downloaded from GSE144000, and we constructed the gene coexpression networks of PM muscle and liver to explore the relationships between WB and the 2 tissues using the weighted gene coexpression network analysis (**WGCNA**) method. Six and 2 gene coexpression modules were significantly correlated with WB in the PM muscle and liver networks, respectively. TGF-beta signaling, Toll-like receptor signaling and mTOR signaling pathways were significantly enriched in the genes within the 6 gene modules of PM muscle network. Meanwhile, mTOR signaling pathway was significantly enriched in the genes within the 2 gene modules of liver network. In the consensus gene coexpression network across the 2 tissues, salmon module ($r = -0.5$ and $p = 0.05$) was significantly negatively correlated with WB, in which Toll-like receptor signaling, apoptosis, and autophagy pathways were significantly enriched. The genes related with the 3 pathways, myeloid differentiation primary response 88 (***MYD88***), interferon regulatory factor 7 (***IRF7***), mitogen-activated protein kinase 14 (***MAPK14***), FBJ murine osteosarcoma viral oncogene homolog (***FOS***), jun proto-oncogene (***JUN***), *caspase-10*, unc-51 like autophagy activating kinase 2 (***ULK2***) and serine/threonine kinase 11 (***LKB1***), were identified in salmon module. In this current study, we found that the signaling pathways related with cell inflammation, apoptosis and autophagy might influence WB across 2 tissues in broilers.

Key words: wooden breast, WGCNA, inflammation, apoptosis, autophagy

2024 Poultry Science 103:104056
https://doi.org/10.1016/j.psj.2024.104056

INTRODUCTION

To meet the growing demand for chicken products, commercial broilers have been bred for fast growth and high breast yield. In the fast-growing and high breast yield broilers, several pectoral myopathies, such as wooden breast (**WB**), have been observed and studied for around ten years (Velleman, 2020; Soglia, et al., 2021). Macroscopically, WB is characterized by palpable firmness of pectoralis major (**PM**) muscle, pale color and ridge-like bulge on caudal area of fillet (Sihvo, et al., 2014; Sihvo, et al., 2018). Due to its visual aspect, rubbery texture, reduction of nutritional value and worsening of meat quality, WB muscle is usually disapproved by consumers (Kuttappan, et al., 2016; Petracci, et al., 2019). WB is not only a poultry health problem, but also a significant economic loss in the poultry industry (Xing, et al., 2020). Therefore, it is of economic value to investigate the molecular mechanism of WB in broilers.

In the last few years, studies on the etiology of WB have been carried out. WB is associated with the excessive production of reactive oxygen species (**ROS**) and high oxidative stress (Hasegawa, et al., 2021; Pan, et al., 2021). The enlargement of breast muscle fibers might be a contributing factor of inadequate vascularization, which limited oxygen availability resulting into accumulation of ROS and oxidative stress in breast muscle (Thanatsang, et al., 2020). In addition, it was reported that the expressions of inflammatory cytokines were dysregulated in WB muscle compared with normal muscle, and the upregulation of Toll-like receptors (**TLRs**) and activation of NF-κB signaling pathway participated in

Received April 8, 2024.
Accepted June 27, 2024.

[1]These authors contributed equally to this work.

[2]Corresponding author: huiyuan@neau.edu.cn

WB (Xing, et al., 2021a). The results of genomic and proteomic studies suggested that WB might be related to hypoxia, oxidative stress, intracellular calcium, fat metabolism and apoptosis (Mutryn, et al., 2015; Carvalho, et al., 2023). Although several factors have been reported to be significantly associated with WB, the exact molecular mechanism is still unknown.

It was reported that the expression changes of genes in the early stages of WB were similar to the dysregulation of genes in human metabolic syndrome (Lake, et al., 2019). Liver is an important metabolic organ, and the liver of WB birds exhibited widespread lesions, inflammatory cell infiltration, occasional collagen deposition or fibrosis and intrahepatic hemorrhages (Xing, et al., 2021b). Abnormal expressions of the genes associated with hepatic fibrosis, oxidative stress, inflammation, and apoptosis were detected in the liver of broilers with WB (Phillips, et al., 2020; Xing, et al., 2021a). Furthermore, the imbalance of triglyceride synthesis was found in the muscle and liver of broilers with WB (Maharjan, et al., 2021). These results suggest that the etiology of WB may be a metabolic pathology involving muscle and liver.

In the present study, to explore the relationships between WB and PM muscle and liver, we downloaded the public RNA-seq dataset of PM and liver from normal and WB broilers (GSE144000) and analyzed the gene expression profiles of the 2 tissues. Then we constructed the gene coexpression networks of PM and liver, respectively, and a consensus gene coexpression networks across 2 tissues to identify the genes and pathways involved in WB. Finally, the functional enrichment analysis of genes clustered within gene coexpression modules significantly correlated with WB was performed based on KEGG and GO terms to reveal potential molecular mechanism of WB.

MATERIALS AND METHODS

Data Collection

The aim of the research was to explore the underlying molecular mechanisms of wooden breast across PM muscle and liver. To reduce the influence of genetic and environmental factors, we selected the gene expression profile dataset of PM muscle and liver from the same genetic background and identical rearing conditions. In the current study, the raw reads of GSE144000 dataset were downloaded from Gene Expression Omnibus (**GEO**) database in National Center for Biotechnology Information (**NCBI**) website, and the RNA-seq dataset consists of the 20 PM samples (15 WB and 5 normal) and 15 liver samples (10 WB and 5 normal) from 45 d male broilers (Phillips, et al., 2020). The broilers were fed with *ad libitum* access to a common commercial starter (1−14 d) and grower (14−45 d) diet as well as water (Phillips, et al., 2020).

Preprocessing Sequencing Data

To get high-quality reads for the subsequent analyses, we filtered out the adapter contamination reads, low-quality reads (the percentage of unqualified bases more than 50%), unpaired reads and reads containing more than 10% N using fastp (v0.19.7) software (Chen, et al., 2018). Next, the high-quality reads were subsequently aligned to the Gallus gallus reference genome using HISAT2 (v2.2.0) following the default workflow (Kim, et al., 2015), and postalignment quality was assessed using Qualimap (v2.2.2d) (Garcia-Alcalde, et al., 2012). Then, based on the count of alignment reads, the expression level of each gene was calculated using FeatureCounts (v2.0.1) software (Liao, et al., 2014). The files of reference genome sequence and annotation were downloaded from the NCBI genome assembly website (ftp://ftp.ncbi.nlm.nih.gov/genomes/all/GCF/000/002/315/GCF_000002315.6_GRCg6a/). A summary of the RNA-Seq datasets, QC, and mapping is provided in Supplementary Table S1.

Analyses of Differentially Expressed Genes

The filterByExpr function of the EdgeR package (v3.24.3) was employed to filter the low expression genes (Robinson, et al., 2010). The principal component analysis (PCA) was performed using the prcomp function of R base (v4.3.1). Based on negative binomial generalized linear models, the differentially expressed genes (**DEGs**) between WB and normal of each tissue were analyzed using DESeq2 (v1.22.2) (Love, et al., 2014). The significant DEGs were identified with the *P*-value lower than 0.05 and absolute logarithmic fold change higher than 0.585, and listed in Supplementary Table S2.

Gene Coexpression Network Construction With WGCNA

In the present study, the gene coexpression networks were constructed using WGCNA package (v1.70) in R (v4.0.5) (Langfelder and Horvath, 2008). According to the criterion of approximate scale-free topology, the optimal soft threshold (power) was set to 14 for further analysis. The blockwiseConsensusModules function of WGCNA package was utilized to construct a consensus gene coexpression network across PM and liver. The minimum number of genes in a module was set to 30, the module detection sensitivity (deepSplit) was set to 2, and the mergeCutHeight parameter was set to 0.2. Finally, we calculated the correlation between the modules and WB to identify significant modules. The blockwiseModules function of WGCNA package was utilized to construct gene coexpression networks of liver and PM, separately, to identify modules which was highly related to WB in each tissue. The optimal soft threshold (power) was set to 18, and minModuleSize was set to 30, and mergeCutHeight was set to 0.15.

Correlation Analysis Between Modules and WB Trait

Module eigengene (**ME**) represents the first principal component of a gene module (Langfelder and Horvath,

2007). To identify gene modules associated with WB, the correlation between ME of each module and WB was calculated using Pearson correlation of WGCNA package. The gene modules with *P*-value less than 0.05 were considered significantly correlated with WB for functional enrichment analysis.

Detection of Tissue-Specific Genes in PM Muscle and Liver

Due to only PM muscle and liver in the current study, we identified tissue-specific genes in the target tissue relative to another tissue with the more simplified criteria based on Zhang's study (Zhang, et al., 2022). The reads of each gene in 15 PM muscle and 10 liver samples with WB were converted to FPKM values. Then, the tissue-specific genes were screened based on the following simplified criteria: the average FPKM value of the candidate gene in the target tissue was more than 3 times that in another tissue, and the expression level of candidate gene ranked in the top 25% in the target tissue.

Functional Enrichment Analyses of Genes Within Gene Modules

To investigate the roles of genes in influencing WB, the functional enrichment analyses of genes in each of modules significantly correlated with WB were performed using clusterProfiler package (v4.4.2) with default parameters (Yu, et al., 2012). The biological pathways and functional annotation of genes were enriched based on the Kyoto Encyclopedia of Genes and Genomes (**KEGG**) database and Gene Ontology (**GO**) categories, and *P*-value ≤ 0.05 was statistically significant.

The PPI Network Construction and Hub Genes Screening

The STRING database (v12.0) (https://cn.string-db.org/) was used to build the protein-protein interaction (**PPI**) network of the genes in modules significantly correlated with WB. A combined score $\geq$0.85 was considered as significant to construct a PPI network. The network graph was visualized and analyzed using Cytoscape (v3.6.0). Hub genes were identified using the CytoHubba-MCC plugin with default parameters (Chin, et al., 2014).

RESULTS

Overview of Preprocessed RNA-Seq Data

The average number of raw reads across 35 samples was 6.99M (2.27M−11.7M, Supplementary Table S1). The average number of high-quality reads was 6.92M (2.27M−11.85M) after filtering out low-quality reads. The average percentage of high-quality reads mapping uniquely to the chicken reference genome was 93.78%, among which exonic regions, intergenic regions and intergenic regions accounted for 80.53%, 13.46% and 6.01%, respectively (Supplementary Table S1).

Differentially Expressed Gene Analyses

PCA analysis revealed that PM muscle and liver samples had a clear separation (Figure 1A). Total 1,062 and 636 significant DEGs in the WB vs normal broilers were identified in PM muscle and liver, respectively (Supplementary Table S2). Total 73 significant DEGs were detected in both comparisons, while 989 and 563 genes were uniquely significantly differentially expressed in PM muscle and liver, respectively (Figure 1B).

In the PM muscle, there were 788 upregulated and 274 downregulated genes in the WB vs normal broilers (Figure 1C). Transforming growth factor beta 1 (***TGFB1***), transforming growth factor beta 2 (***TGFB2***), transforming growth factor beta 3 (***TGFB3***), interleukin 11 (***IL11***), toll-like receptor 2 family member A (***TLR2A***), toll-like receptor 4 (***TLR4***), all of which were significantly upregulated in the PM muscle of WB broilers compared to that of normal broilers (Figure 1C). Growth arrest specific 6 (***GAS6***), glutaredoxin (***GLRX***), ankyrin repeat and SOCS box containing 4 (***ASB4***), interleukin 11 (***IL11***), SMAD family member 9 (***SMAD9***), all of which were significantly downregulated in the PM muscle of WB broilers compared to that of normal broilers (Figure 1C).

In the liver, there were 450 upregulated and 186 downregulated genes in the WB vs normal broilers (Figure 1D). Dimethylarginine dimethylaminohydrolase 1 (***DDAH1***), actin alpha 2, smooth muscle (***ACTA2***), all of which were significantly upregulated in the liver of WB broilers compared to that of normal broilers (Figure 1D). Carnitine palmitoyltransferase 1A (***CPT1A***), forkhead box N3 (***FOXN3***), apolipoprotein F (***APOF***), all of which were significantly downregulated in the liver of WB broilers compared to that of normal broilers (Figure 1D).

Construction of Gene Coexpression Networks and Analysis of Correlations Between Gene Modules and WB in Liver and PM Muscle

After filtering out genes with low expression levels, there were 10,758 genes used to construct a gene coexpression network of PM muscle, and 33 gene coexpression modules (without grey module) were clustered (Figure 2A). The correlations between each gene module and WB were calculated, and 6 modules were significantly correlated with WB in PM muscle (Figure 2C). Darkolivegreen module had the highest association with WB ($r = 0.64$ and $p = 0.002$), and turquoise module contained the highest number of genes (1381 genes) among the 6 gene modules significantly correlated WB. Among the genes within modules significantly correlated with WB, 263 tissue-specific genes in muscle relative to liver

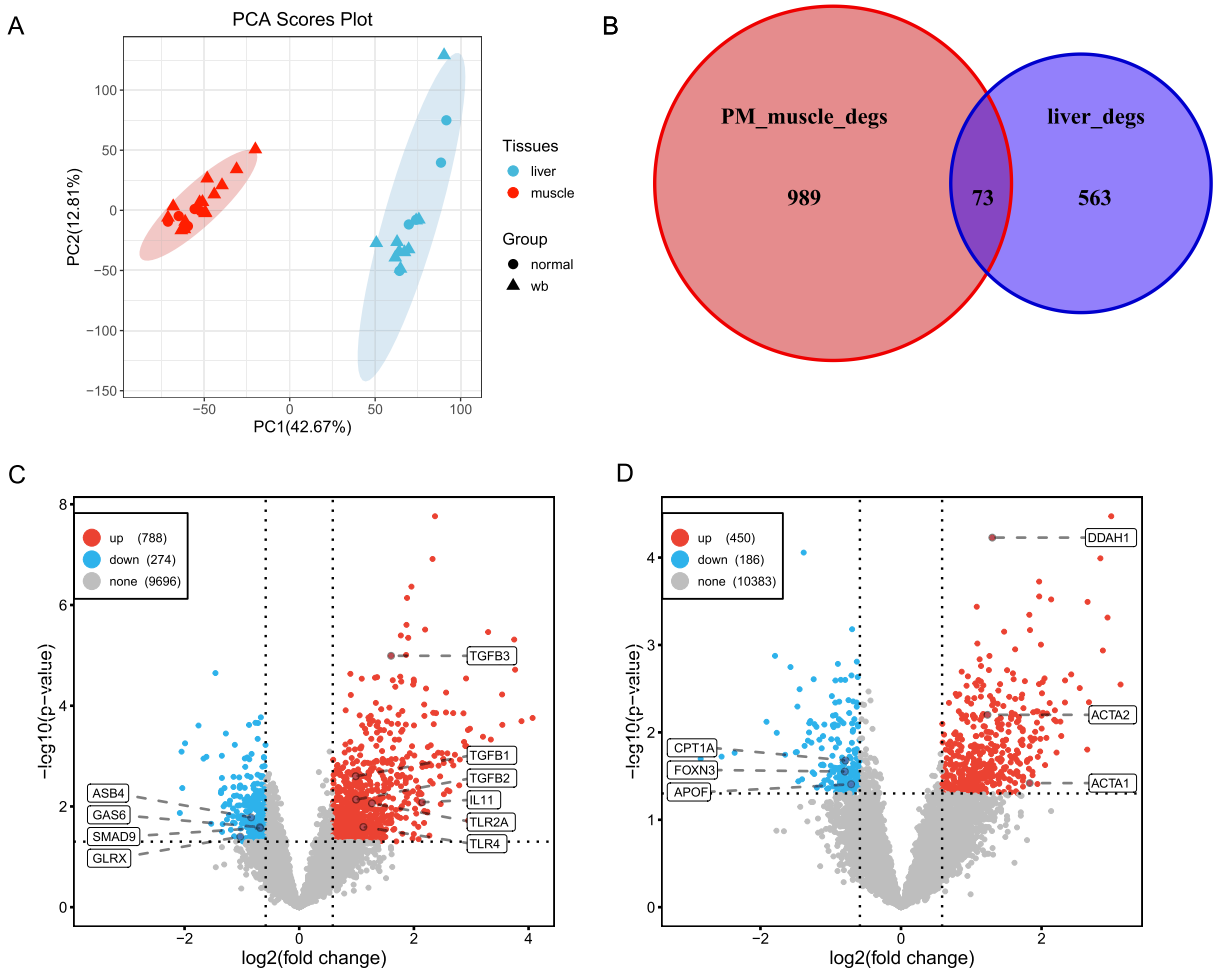

Figure 1. (A) PCA analysis of PM muscle and liver samples. Red and blue indicate PM muscle and liver, respectively. Dot and triangle represent normal and WB samples. (B) Volcano map of differentially expressed genes in PM muscle between WB and normal group. (C) Volcano map of differentially expressed genes in liver between WB and normal group. The horizontal axis represents log2 (fold change), while the vertical axis represents -log10 (*P*-value). The blue dots indicate downregulated genes, while the red dots represent upregulated genes within WB compared with normal group. (D) Venn diagram of differentially expressed genes overlapping in PM muscle and liver. Red circle means PM muscle and blue circle means liver.

were identified (Supplementary Table S3). In the 263 genes, myosin heavy chain 1B, skeletal muscle (***MYH1B***), myosin heavy chain 1C, skeletal muscle (***MYH1C***), myosin heavy chain 1D, skeletal muscle (***MYH1D***), myosin heavy chain 1E, skeletal muscle (***MYH1E***), and myosin heavy chain 1G, and skeletal muscle (***MYH1G***) are relevant to the development of skeletal muscle fibers, and *TGFB1, TGFB2*, and *TGFB3* are associated with the development of endomysial fibrosis.

In addition, 11,019 genes were used to construct a gene coexpression network of liver, and 26 gene coexpression modules (without grey module) were clustered (Figure 2B). The correlations between each gene module and WB trait were calculated, and 2 modules significantly correlated with WB were detected in liver (Figure 2D). Dark red module was found to have the highest association with WB (r = 0.58 and p = 0.02), and light cyan module had the highest number of genes (142 genes) among the 2 gene modules significantly correlated WB. Among genes within modules significantly correlated with WB, 26 tissue-specific genes in liver relative to PM muscle were identified (Supplementary Table S3). Hepatocyte nuclear factor 4 alpha (***HNF4A***) is relevant growth and differentiation of liver cell and *ACTA2* is associated with the development of fibrosis.

Functional Enrichment Analyses of Gene Modules

Based on the KEGG and GO databases, 133 KEGG pathways and 1409 GO terms were significantly enriched in the gene modules of PM muscle (Supplementary Tables S4 and S5). TGF-beta signaling pathway was significantly enriched in the genes within dark olive green, dark orange and green modules of PM muscle, and 3 relevant genes of the pathway, *TGFB1, TGFB2* and *TGFB3*, were identified in the dark olive green and

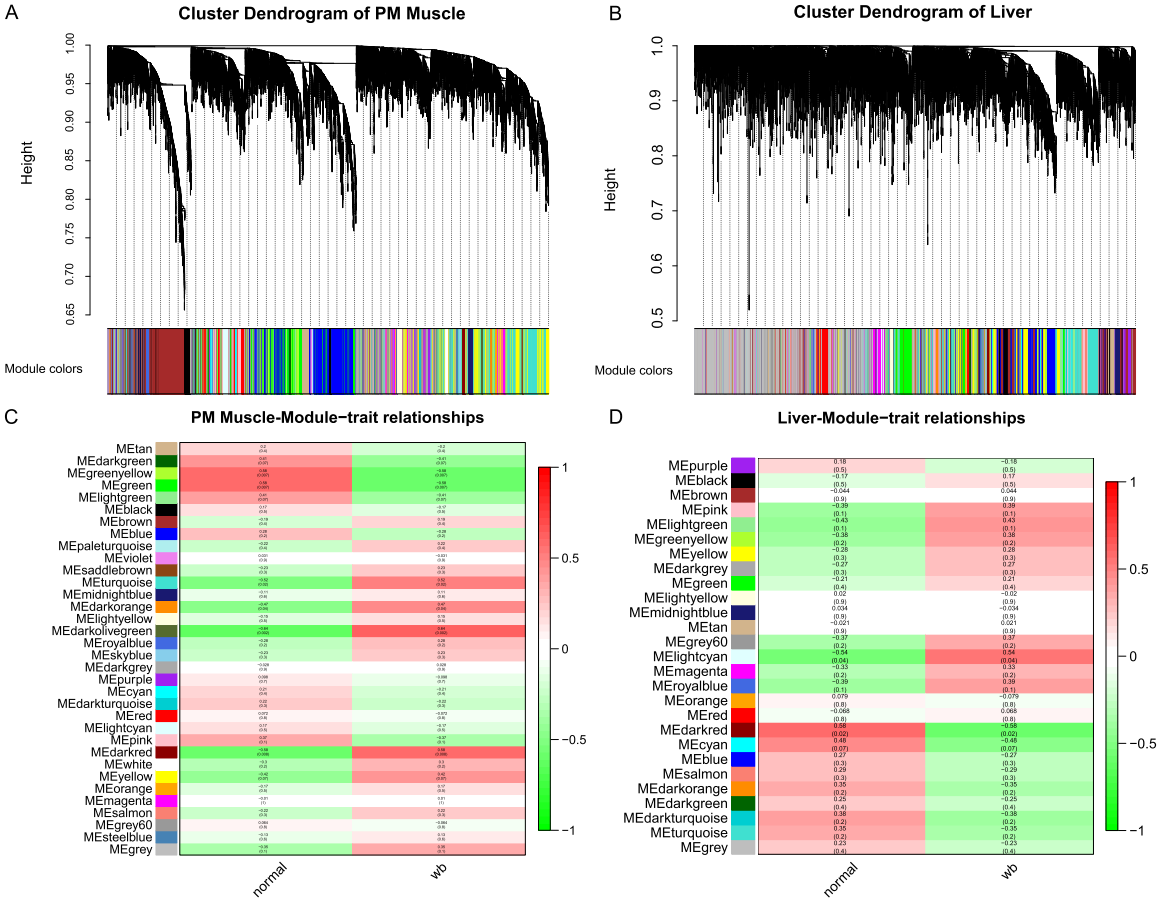

Figure 2. Cluster of coexpression genes and analyses of correlation between gene modules and WB. (A) The cluster dendrogram of coexpression genes in PM muscle network. (B) The cluster dendrogram of coexpression genes in liver network. Each color represents a gene coexpression module. (C) The correlation between each gene module and WB in PM muscle network. (D) The correlation between each gene module and WB in liver network. Each row corresponds to a gene module, and each column represents a trait. Each cell contains the corresponding correlation and *p*-value.

turquoise modules (Supplementary Table S4). Toll-like receptor signaling pathway was significantly enriched in the turquoise module of PM muscle, and relevant genes of the pathway, myeloid differentiation primary response 88 (***MYD88***), *TLR2A*, mitogen-activated protein kinase 14 (***MAPK14***), Fas associated via death domain (***FADD***), *TLR4* and signal transducer and activator of transcription 1 (***STAT1***), were identified (Supplementary Table S4). GO terms related to the fibroblast, such as cellular response to fibroblast growth factor stimulus, negative regulation of fibroblast proliferation, myofibril assembly, and positive regulation of fibroblast apoptotic process, were significantly enriched in the darkorange, darked and turquoise modules of PM muscle (Supplementary Table S5).

Total 19 pathways and 397 GO terms were significantly enriched in the gene modules of liver (Supplementary Tables S6 and S7). MAPK signaling pathway was significantly enriched in the darkred module of liver, and relevant genes, heat shock protein family A member 2 (***HSPA2***) and mitogen-activated protein kinase kinase kinase 14 (***MAP3K14***), were identified (Supplementary Table S6). GO terms related to the mitochondrial such as mitochondrial fragmentation involved in apoptotic process, apoptotic mitochondrial changes, and mitochondrial transmembrane transport, were significantly enriched in the darkred and lightcyan modules of liver (Supplementary Table S7).

Construction of Consensus Network and Analysis of Correlation Between Consensus Modules and WB

Total 9,539 genes expressed across PM muscle and liver and were used to construct a consensus gene coexpression network across the 2 tissues with the optimal soft threshold (power) set to 14 (Figure 3). A total of 30 consensus modules (without grey module) were detected in the consensus gene coexpression network (Figure 4A). The results showed that 30 consensus modules could be clustered into 2 clusters in PM muscle (Figure 5A) and liver (Figure 5B) networks, and heatmaps showed similar results (Figures 5C and F). The high-density value D = 0.66 reflected the overall preservation between the 2 tissues networks (Figure 5D). The adjacency heatmap presented the preservation network between muscle and liver eigengene networks (Figure 5E). A total of 14 modules were retained, and salmon consensus module was highly correlated with WB with correlation coefficient = −0.5 and *P*-value = 0.05 (Figure 4B).

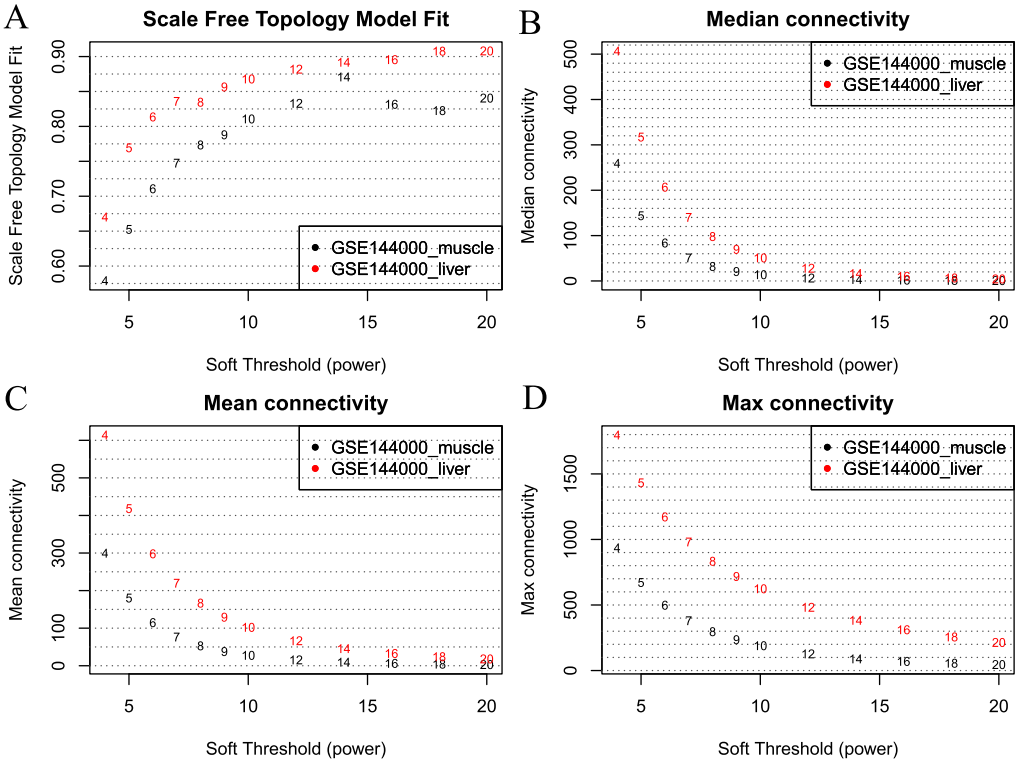

Figure 3. Analysis of network topology for various soft-thresholding powers. (A) network construction was provided by calculating the scale-free topology fit index of several powers. The x-axis represents the soft-thresholding power and the y-axis represents the scale-free fit index. Fourteen was chosen as the appropriate soft threshold. (B) Mean connectivity of a weighted network. (C) Median connectivity of a weighted network. (D) Maximum connectivity of a weighted network.

Functional Enrichment Analyses of Consensus Gene Modules

The salmon consensus module contained 293 genes (Table 1), in which 18 pathways and 103 GO terms were significantly enriched. In the 18 biological pathways, programmed cell death-related pathways were enriched, such as apoptosis, non-homologous end-joining, autophagy - animal and necroptosis, and relevant genes of these pathways, unc-51 like autophagy activating kinase 2 (***ULK2***), serine/threonine kinase 11 (***STK11***), caspase 10, apoptosis-related cysteine peptidase (***CASP10***), FBJ murine osteosarcoma viral oncogene homolog (***FOS***), jun proto-oncogene (***JUN***), signal transducer and activator of transcription 6 (***STAT6***), *STAT1*, growth arrest and DNA-damage-inducible, alpha (***GADD45A***) and growth arrest and DNA damage inducible gamma (***GADD45G***) were identified (Figure 6A). Cell stress related terms were enriched, such as response to stress, DNA repair, cellular response to DNA damage stimulus, cellular response to stress, were significantly enriched (Figure 6B).

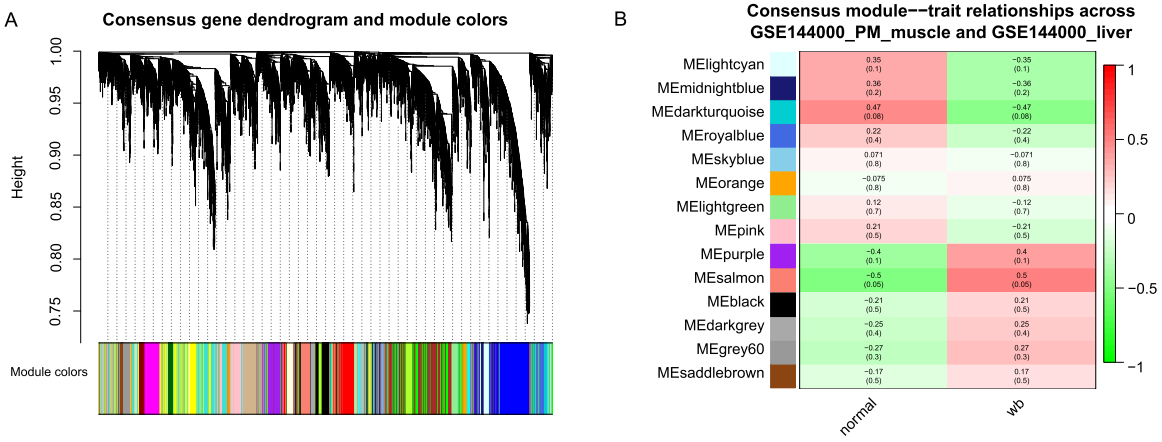

Figure 4. Cluster of coexpression genes and analyses of correlation between each consensus gene module and WB across PM muscle and liver. (A) The cluster dendrogram of coexpression genes across 2 tissues. (B) The correlation between each gene module and WB across 2 tissues. Each row corresponds to a consensus gene module, and column corresponds to a trait. Each cell contains the corresponding correlation and *P*-value.

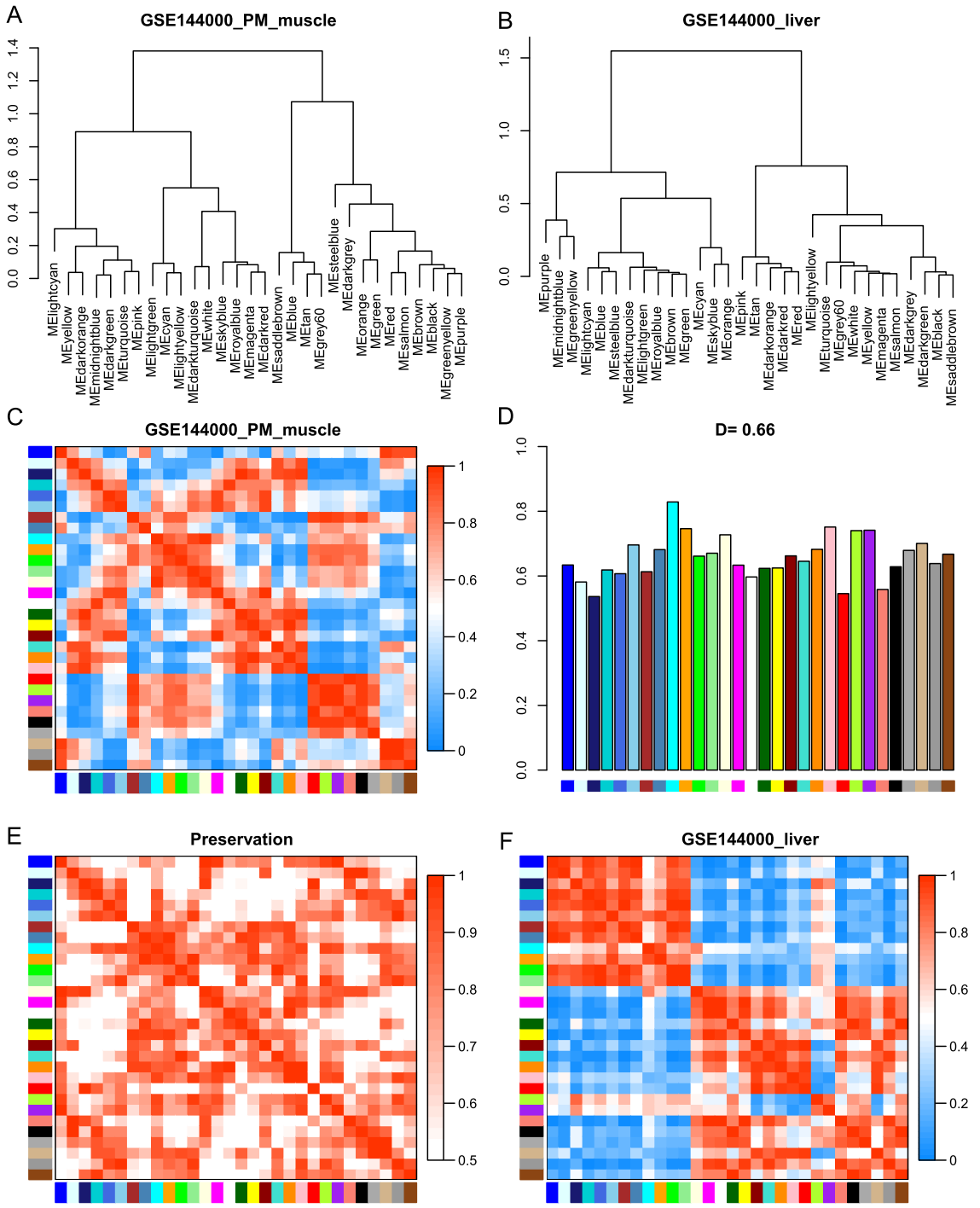

Figure 5. Differential eigengene network analyses across 2 tissues. The dendrograms (clustering trees) of the consensus module eigengenes in PM muscle (A) and liver (B). Heatmaps of consensus module eigengene adjacencies in PM muscle (C) and liver (F). Each row and column represent a consensus module eigengene. Red indicates high adjacency (positively correlation), and blue indicates low adjacency (negatively correlation) within the heatmap. Adjacency heatmap for PM muscle and liver preservation network (E). Each row and column represent a consensus module eigengene. Red indicates high adjacency (positively correlation), and white indicates low adjacency (negatively correlation) within the heatmap. Barplot of the average preservation of adjacency between each eigengene and all other eigengenes (D). The barplot representing the column means of the preservation heatmap. The density value D = 0.66 reflects overall network preservation.

Construction of PPI Network and Identification of Key Genes

Based on the STRING database, the PPI network of genes within salmon consensus module was constructed with setting the minimum required interaction score = 0.85. After removing unconnected nodes, a PPI network was successfully constructed with 81 nodes and 94 edges (Figure 7). Furthermore, we detected hub genes from the network using MCC function of Cytoscape, and the MCC value of gene was higher than 10, which was considered as hub genes in current study. The 15 hub genes were suppressor of cytokine signaling 3 (***SOCS3***), heme oxygenase 1 (***HMOX1***), interferon induced, with

Table 1. Summary of consensus modules across 2 tissues.

Modules	Gene count	Modules	Gene count	Modules	Gene count
lightcyan	179	cyan	216	turquoise	902
grey	639	green	605	lightgreen	154
grey60	167	brown	825	darkred	151
royalblue	151	darkgrey	130	lightyellow	152
greenyellow	301	black	345	white	98
midnightblue	208	darkorange	99	darkgreen	148
steelblue	51	magenta	336	darkturquoise	138
pink	340	orange	126	saddlebrown	82
purple	325	yellow	771	skyblue	87
salmon	293	tan	298		
blue	845	red	377		

helicase C domain 1(***IFIH1***), tyrosine kinase 2 (***TYK2***), *MAPK14*, early growth response 1 (***EGR1***), *FOS*, interferon regulatory factor 7 (***IRF7***), cadherin 2, type 1, N-cadherin (neuronal) (***CDH2***), STAT1, fibronectin 1(***FN1***), *JUN*, catenin (cadherin-associated protein), delta 1 (***CTNND1***), ubiquitin specific peptidase 18 (***USP18***) and interferon alpha and beta receptor subunit 1 (***IFNAR1***), which were highlighted in red in the Figure 7.

DISCUSSION

Fibrosis is a prominent pathological feature of wood breast (WB) myopathy in broilers (Sihvo, et al., 2014). Fibrosis and varying degrees of necrotic fibers appeared in the PM muscle, and some fibrotic sites were also observed in the liver of broilers with WB (Oliveira, et al., 2021; Xing, et al., 2021b). In the current study, TGF-β singling pathway was significantly enriched in the dark olive green, green, and dark orange modules of PM muscle network. Relevant genes of TGF-β singling pathway, *TGFB1, TGFB2* and *TGFB3*, were identified in the 3 modules, and the 3 genes were significantly upregulated in the PM muscle of WB group compared with those in normal group. TGF-β plays an important role in the pathogenesis of fibrotic disorders and is the master regulator of fibrosis (Ismaeel, et al., 2019). In the PM muscle of WB broilers, the activation of TGF-β signaling could initiate the downstream signaling transduction and enhance ECM protein deposition to induce severe fibrosis (Xing, et al., 2021c). The mRNA expression levels of 3 TGF-β isoforms, *TGF-β1, TGF-β2,* and *TGF-β3* in the PM muscle affected by WB were significantly higher and the relative content of TGF-β protein in the WB group exhibited a significantly higher compared to

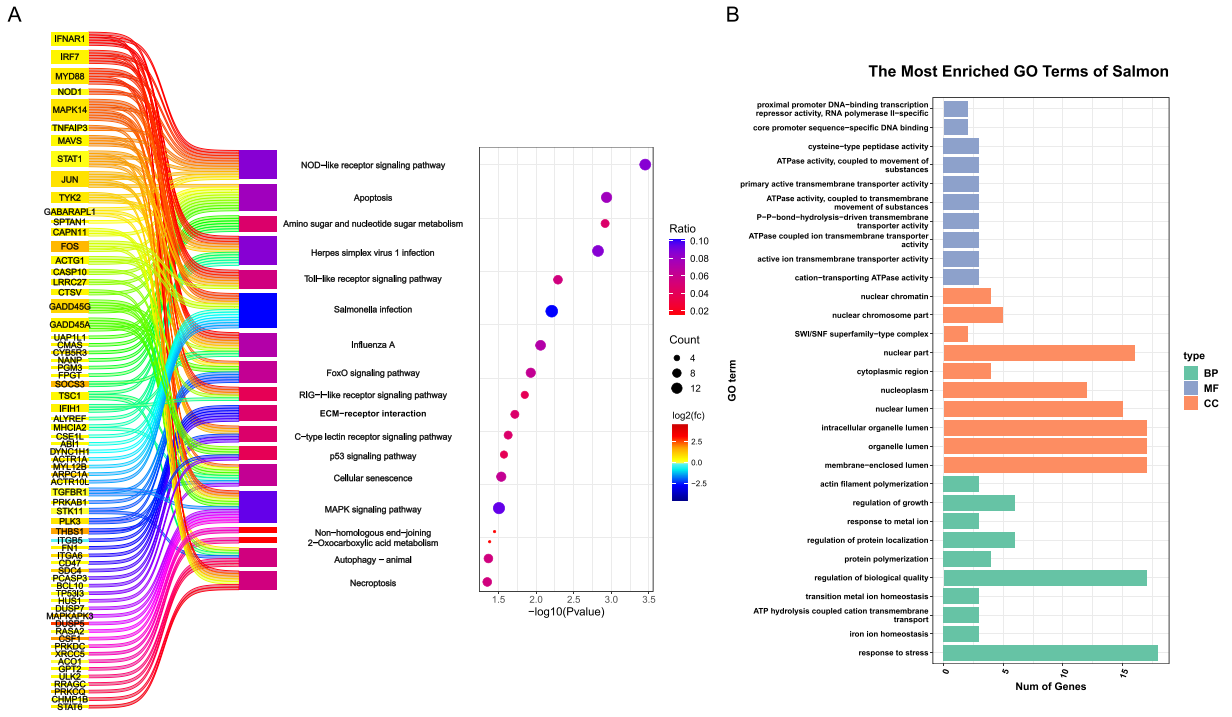

Figure 6. (A) A combination of the bubble plot and the Sankey diagram demonstrating statistically significant KEGG pathways. The y-axis of the Sankey diagram shows the genes within each pathway. The color of the genes represents log2 (fold change), and the color of the pathway represents the ratio of gene enriched in this pathway, the same as the color of the bubble plot. The x-axis of the bubble plot shows the −log10 (*P*-value) of KEGG enrichment significance. The point size represents number of genes enriched in this pathway. (B) Functional enrichment analysis of genes within coexpression modules based on GO terms. The x-axis shows the number of genes enriched in this GO term. The 3 colors represent the 3 types of GO terms.

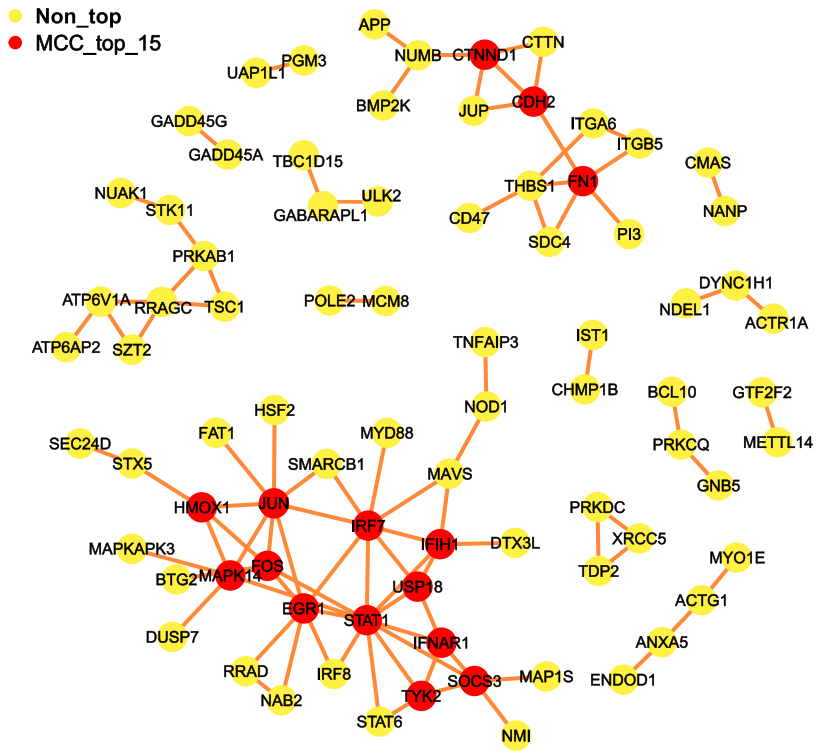

Figure 7. Construction of PPI network. The PPI network of genes within the salmon consensus module was analyzed, and top 15 genes were identified according to MCC value, which were highlighted in red.

the normal group (Xing, et al., 2021c). In this current study, *TGFB3* and *ACTA2* were detected in the dark red and light cyan modules of liver network, and the 2 genes were significantly upregulated in the liver of WB group than those in the normal group. As a hallmark gene of tissue fibrogenesis, the up-regulation of alpha-smooth muscle actin (**α-SMA**) encoded by *ACTA2* was detected in the fibrotic liver compared with normal liver (Gieling, et al., 2009; Xu, et al., 2016). In the current study, ECM-receptor interaction pathway was significantly enriched in the salmon consensus module across 2 tissues, in which *FN1* was identified. *FN1* encoded fibronectin which was used as myofibrotic marker to assess fibrosis (Vukotić, et al., 2022). In the PM muscle, the expression of FN1 was significantly upregulated in WB broilers than it in control broilers (Praud, et al., 2020). The process of hepatic fibrosis involves the trans activation of hepatic stellate cells or portal fibroblasts, leading to their transformation into myofibroblasts. As hepatic stellate cell activators, FN1 participated in the fibrosis pathways in liver (Aseem, et al., 2021).

Immune cell infiltration is a histopathological hallmark of the WB myopathy, and inflammatory response changes with the progression of WB (Xing, et al., 2021a). In the turquoise module of PM muscle network, *TLR2A, TLR4* and *IL-11* were identified and significantly enriched in Toll-like receptor signaling pathway. The mRNA levels and protein levels of *TLR2* and *TLR4* were significantly higher in the WB group than control group (Xing, et al., 2021a). IL-11 had pro-fibrotic activity in fibroblasts and stimulated fibroblasts to secret pro-inflammatory factors (Widjaja, et al., 2022). In the light cyan module of liver network, *DDAH1* was significantly upregulated in the WB group than it in the normal group. The degree of hepatic dysfunction correlated with levels of Asymmetric-dimethylarginine (ADMA) degraded by DDAH1 in liver (Mookerjee, et al., 2015). Severe inflammation and oxidative stress led to impaired activity of DDAH1, resulting in raised ADMA concentrations in the dysfunctional liver (Ferrigno, et al., 2015). Conversely, increase of DDAH1 can attenuate ADMA accumulation in liver (Ferrigno, et al., 2015; Mookerjee, et al., 2015). In the salmon module of consensus network, *MyD88, IRF7, MAPK14, JUN* and *FOS* were significantly enriched in Toll-like receptor signaling pathway and also were hub genes in the PPI network. MyD88 plays a crucial role of Toll-like signaling pathway, and is used by almost all Toll-like receptors to mediate inflammatory responses (Kawasaki and Kawai, 2014; Chen, et al., 2020). IRF7 is a key transcription factor involved in the activation of the type I interferon response inflammatory, which activation can occur by MyD88-dependent pathways (O'Neill, 2006). *MAPK14* is one of stress-activated MAPKs, that regulates inflammatory cytokine expression (Cuadrado and Nebreda, 2010; Hotamisligil and Davis, 2016). The dimeric complex AP-1 is an important transcription factor, which primarily consists of FOS and JUN family members (Sawai, et al., 2013). AP-1 was activated by phosphorylated p38 and regulated expression of inflammatory genes (Yang, et al., 2014).

Apoptosis was induced by WB myopathy in the liver and muscle of broiler chickens (Greene, et al., 2023; Xing, et al., 2021b). Apoptosis is enabled as an organic defense mechanism when cells are damaged in the setting of tissue injury (Elmore, 2007). In the network of

PM muscle, the apoptosis pathway was significantly enriched in the turquoise and green modules, in which *BID* and *FADD* were identified. As a critical substrate of caspase-8, BID is essential for initiation of stress-induced apoptosis (Strasser, et al., 2009). During the process of inducing apoptosis, FADD played an important role in recruitment and activation of caspase-8 and caspase-10 (Sprick, et al., 2002). In the current study, *NFKBIA* was detected in the magenta module of liver network. NFKBIA was an inhibitor of κB to control NF-κB signaling pathway activation (Zhang, et al., 2005). NF-κB is involved in protection of hepatic stellate cells from apoptosis (Sun and Karin, 2008). In addition to inhibiting NF-κB, NFKBIA also prevents apoptosis through protecting the integrity of the outer mitochondrial membrane and controlling the mitochondrial pathway for apoptosis (Pazarentzos, et al., 2014). In the salmon module of consensus network, caspase-10 was significantly enriched in apoptosis pathway. The apoptosis process was induced by over-expression of caspase-10 (Kischkel, et al., 2001). Autophagy is a controlled self-degradation process of cellular components, which plays a crucial role in maintaining cellular homeostasis (He and Klionsky, 2009). In the current study, *ULK2* and *LKB1* were identified in the salmon module and were significantly enriched in autophagy pathway. There might be a relationship between altered autophagy and WB, and autophagosomes were observed in the cytosol of the myoblasts in WB (Hosotani, et al., 2020). Ulk1/2 phosphorylated Atg13, FIP200 and itself, and activated autophagosome formation (Alers, et al., 2012; Mizushima, 2010). LKB1 triggered autophagy through phosphorylating and activating AMPK (Liang, et al., 2021). Therefore, we inferred that an initiation of both apoptosis and autophagy might be associated with WB in broilers.

CONCLUSIONS

In this current study, we constructed gene coexpression networks of pectoralis major (**PM**) muscle, liver and across 2 tissues, respectively, and identified gene modules significantly associated with WB. In the modules significantly correlated with WB of 3 networks, fibrosis-related pathway was significantly enriched and the genes relevant fibrosis, *TGFB1, TGFB2*, and *TGFB3* in muscle tissue, *ACTA2* and *TGFB3* in liver tissue, and *FN1* in both tissues, were identified. The results were suggested that PM muscle and liver might share underlying some molecular pathways, but different genes participated in these pathways between the 2 tissues in fibrosis of WB. In the consensus network, Toll-like receptor signaling pathway, apoptosis pathway and autophagy pathway were significantly enriched, and the genes relevant apoptosis and autophagy, *MyD88, IRF7, MAPK14, FOS, JUN, caspase-10, ULK2* and *LKB1* were identified. These results showed that inflammation and programmed cell death might play an important role in the WB. In summary, the study investigated the genes and pathways associated with WB across PM muscle and liver using WGCNA method and provided an integrative analysis idea on across multiple tissues for understanding WB.

ACKNOWLEDGMENTS

This research was supported by Heilongjiang Provincial Natural Science Foundation of China (LH2023C014).

DISCLOSURES

The authors declare that they have no conflict of interest.

SUPPLEMENTARY MATERIALS

Supplementary material associated with this article can be found in the online version at doi:10.1016/j.psj.2024.104056.

REFERENCES

Alers, S., A. S. Löffler, S. Wesselborg, and B. Stork. 2012. Role of AMPK-mTOR-Ulk1/2 in the regulation of autophagy: Cross talk, shortcuts, and feedbacks. Mol. Cell. Biol. 32:2–11.

Aseem, S. O., N. Jalan-Sakrikar, C. Chi, A. Navarro-Corcuera, T. M. De Assuncao, F. H. Hamdan, S. Chowdhury, J. M. Banales, S. A. Johnsen, V. H. Shah, and R. C. Huebert. 2021. Epigenomic evaluation of cholangiocyte transforming growth factor-beta signaling identifies a selective role for histone 3 lysine 9 acetylation in biliary fibrosis. Gastroenterology 160 889-905 e810.

Carvalho, L. M., T. C. Rocha, J. Delgado, S. Díaz-Velasco, M. S. Madruga, and M. Estévez. 2023. Deciphering the underlying mechanisms of the oxidative perturbations and impaired meat quality in Wooden breast myopathy by label-free quantitative MS-based proteomics. Food Chem. 423:136314.

Chen, L., L. Zheng, P. Chen, and G. Liang. 2020. Myeloid differentiation primary response protein 88 (MyD88): The central hub of TLR/IL-1R signaling. J Med Chem 63:13316–13329.

Chen, S., Y. Zhou, Y. Chen, and J. Gu. 2018. fastp: an ultra-fast all-in-one FASTQ preprocessor. Bioinformatics 34:i884–i890.

Chin, C. H., S. H. Chen, H. H. Wu, C. W. Ho, M. T. Ko, and C. Y. Lin. 2014. CytoHubba: identifying hub objects and sub-networks from complex interactome. BMC Syst. Biol. 8:S11.

Cuadrado, A., and A. R. Nebreda. 2010. Mechanisms and functions of p38 MAPK signalling. Biochem. J. 429:403–417.

Elmore, S. 2007. Apoptosis: A review of programmed cell death. Toxicol. Pathol. 35:495–516.

Ferrigno, A., L. G. Di Pasqua, C. Berardo, P. Richelmi, and M. Vairetti. 2015. Liver plays a central role in asymmetric dimethylarginine-mediated organ injury. World J. Gastroenterol. 21:5131–5137.

Garcia-Alcalde, F., K. Okonechnikov, J. Carbonell, L. M. Cruz, S. Gotz, S. Tarazona, J. Dopazo, T. F. Meyer, and A. Conesa. 2012. Qualimap: Evaluating next-generation sequencing alignment data. Bioinformatics 28:2678–2679.

Gieling, R. G., K. Wallace, and Y. P. Han. 2009. Interleukin-1 participates in the progression from liver injury to fibrosis. Am. J. Physiol. Gastrointest. Liver Physiol. 296:G1324–G1331.

Greene, E. S., C. Maynard, G. Mullenix, M. Bedford, and S. Dridi. 2023. Potential role of endoplasmic reticulum stress in broiler woody breast myopathy. Am. J. Physiol. Cell. Physiol. 324:C679–C693.

Hasegawa, Y., T. Kawasaki, N. Maeda, M. Yamada, N. Takahashi, T. Watanabe, and T. Iwasaki. 2021. Accumulation of lipofuscin in broiler chicken with wooden breast. Anim. Sci. J. 92:e13517.

He, C., and D. J. Klionsky. 2009. Regulation mechanisms and signaling pathways of autophagy. Annu. Rev. Genet. 43:67–93.

Hosotani, M., T. Kawasaki, Y. Hasegawa, Y. Wakasa, M. Hoshino, N. Takahashi, H. Ueda, T. Takaya, T. Iwasaki, and T. Watanabe. 2020. Physiological and pathological mitochondrial clearance is related to pectoralis major muscle pathogenesis in broilers with wooden breast syndrome. Front. Physiol. 11:579.

Hotamisligil, G. S., and R. J. Davis. 2016. Cell signaling and stress responses. Cold Spring Harb. Perspect. Biol. 8:a006072.

Ismaeel, A., J. S. Kim, J. S. Kirk, R. S. Smith, W. T. Bohannon, and P. Koutakis. 2019. Role of transforming growth factor-beta in skeletal muscle fibrosis: A review. Int. J. Mol. Sci. 20:2446.

Kawasaki, T., and T. Kawai. 2014. Toll-like receptor signaling pathways. Front. Immunol. 5:461.

Kim, D., B. Langmead, and S. L. Salzberg. 2015. HISAT: a fast spliced aligner with low memory requirements. Nat. Methods. 12:357–360.

Kischkel, F. C., D. A. Lawrence, A. Tinel, H. LeBlanc, A. Virmani, P. Schow, A. Gazdar, J. Blenis, D. Arnott, and A. Ashkenazi. 2001. Death receptor recruitment of endogenous caspase-10 and apoptosis initiation in the absence of caspase-8. J. Biol. Chem. 276:46639–46646.

Kuttappan, V. A., B. M. Hargis, and C. M. Owens. 2016. White striping and woody breast myopathies in the modern poultry industry: a review. Poult Sci 95:2724–2733.

Lake, J. A., M. B. Papah, and B. Abasht. 2019. Increased expression of lipid metabolism genes in early stages of wooden breast links myopathy of broilers to metabolic syndrome in humans. Genes 10:746.

Langfelder, P., and S. Horvath. 2007. Eigengene networks for studying the relationships between co-expression modules. BMC Syst. Biol. 1:54.

Langfelder, P., and S. Horvath. 2008. WGCNA: An R package for weighted correlation network analysis. BMC Bioinformatics 9:559.

Liang, Y., Z. Zhang, J. Tu, Z. Wang, X. Gao, K. Deng, M. A. El-Samahy, P. You, Y. Fan, and F. Wang. 2021. γ-Linolenic acid prevents lipid metabolism disorder in palmitic acid-treated alpha mouse liver-12 cells by balancing autophagy and apoptosis via the LKB1-AMPK-mTOR pathway. J. Agric. Food Chem. 69:8257–8267.

Liao, Y., G. K. Smyth, and W. Shi. 2014. Feature counts: An efficient general purpose program for assigning sequence reads to genomic features. Bioinformatics 30:923–930.

Love, M. I., W. Huber, and S. Anders. 2014. Moderated estimation of fold change and dispersion for RNA-seq data with DESeq2. Genome biology 15:550.

Maharjan, P., A. Beitia, J. Weil, N. Suesuttajit, K. Hilton, J. Caldas, C. Umberson, D. Martinez, B. Kong, C. M. Owens, and C. Coon. 2021. Woody breast myopathy broiler show age-dependent adaptive differential gene expression in Pectoralis major and altered in-vivo triglyceride kinetics in adipogenic tissues. Poult. Sci. 100:101092.

Mizushima, N. 2010. The role of the Atg1/ULK1 complex in autophagy regulation. Curr. Opin. Cell. Biol. 22:132–139.

Mookerjee, R. P., G. Mehta, V. Balasubramaniyan, Z. M. Fel, N. Davies, V. Sharma, Y. Iwakiri, and R. Jalan. 2015. Hepatic dimethylarginine-dimethylaminohydrolase1 is reduced in cirrhosis and is a target for therapy in portal hypertension. J. Hepatol. 62:325–331.

Mutryn, M. F., E. M. Brannick, W. Fu, W. R. Lee, and B. Abasht. 2015. Characterization of a novel chicken muscle disorder through differential gene expression and pathway analysis using RNA-sequencing. BMC Genomics 16:399.

O'Neill, L. A. J. 2006. How Toll-like receptors signal: what we know and what we don't know. Curr. Opin. Immunol. 18:3–9.

Oliveira, R. F., J. L. M. Mello, F. B. Ferrari, E. N. F. Cavalcanti, R. A. Souza, M. R. Pereira, A. Giampietro-Ganeco, E. A. Villegas-Cayllahua, H. A. Fidelis, M. S. Favero, L. Amoroso, P. A. Souza, and H. Borba. 2021. Physical, chemical and histological characterization of pectoralis major muscle of broilers affected by wooden breast myopathy. Animals (Basel) 11:596.

Pan, X., L. Zhang, T. Xing, J. Li, and F. Gao. 2021. The impaired redox status and activated nuclear factor-erythroid 2-related factor 2/antioxidant response element pathway in wooden breast myopathy in broiler chickens. Anim. Biosci. 34:652–661.

Pazarentzos, E., A.-L. Mahul-Mellier, C. Datler, W. Chaisaklert, M.-S. Hwang, J. Kroon, D. Qize, F. Osborne, A. Al-Rubaish, A. Al-Ali, N. D. Mazarakis, E. O. Aboagye, and S. Grimm. 2014. IκBα inhibits apoptosis at the outer mitochondrial membrane independently of NF-κB retention. EMBO J. 33:2814–2828.

Petracci, M., F. Soglia, M. Madruga, L. Carvalho, E. Ida, and M. Estevez. 2019. Wooden-breast, white striping, and spaghetti meat: Causes, consequences and consumer perception of emerging broiler meat abnormalities. Compr. Rev. Food Sci. Food. Saf. 18:565–583.

Phillips, C. A., B. J. Reading, M. Livingston, K. Livingston, and C. M. Ashwell. 2020. Evaluation via supervised machine learning of the broiler pectoralis major and liver transcriptome in association with the muscle myopathy wooden breast. Front. Physiol. 11:101.

Praud, C., J. Jimenez, E. Pampouille, N. Courousse, E. Godet, E. L.e Bihan-Duval, and C. Berri. 2020. Molecular phenotyping of white striping and wooden breast myopathies in chicken. Front. Physiol. 11:633.

Robinson, M. D., D. J. McCarthy, and G. K. Smyth. 2010. edgeR: a Bioconductor package for differential expression analysis of digital gene expression data. Bioinformatics 26:139–140.

Sawai, M., Y. Ishikawa, A. Ota, and H. Sakurai. 2013. The proto-oncogene JUN is a target of the heat shock transcription factor HSF1. FEBS J. 280:6672–6680.

Sihvo, H. K., N. Airas, J. Linden, and E. Puolanne. 2018. Pectoral vessel density and early ultrastructural changes in broiler chicken wooden breast myopathy. J. Comp. Pathol. 161:1–10.

Sihvo, H. K., K. Immonen, and E. Puolanne. 2014. Myodegeneration with fibrosis and regeneration in the pectoralis major muscle of broilers. Vet. Pathol. 51:619–623.

Soglia, F., M. Petracci, R. Davoli, and M. Zappaterra. 2021. A critical review of the mechanisms involved in the occurrence of growth-related abnormalities affecting broiler chicken breast muscles. Poult. Sci. 100:101180.

Sprick, M. R., E. Rieser, H. Stahl, A. Grosse-Wilde, M. A. Weigand, and H. Walczak. 2002. Caspase-10 is recruited to and activated at the native TRAIL and CD95 death-inducing signalling complexes in a FADD-dependent manner but can not functionally substitute caspase-8. EMBO J. 21:4520–4530.

Strasser, A., P. J. Jost, and S. Nagata. 2009. The many roles of FAS receptor signaling in the immune system. Immunity 30:180–192.

Sun, B., and M. Karin. 2008. NF-kappaB signaling, liver disease and hepatoprotective agents. Oncogene 27:6228–6244.

Thanatsang, K. V., Y. Malila, S. Arayamethakorn, Y. Srimarut, N. Tatiyaborworntham, T. Uengwetwanit, A. Panya, W. Rungrassamee, and W. Visessanguan. 2020. Nutritional properties and oxidative indices of broiler breast meat affected by wooden breast abnormality. Animals (Basel) 10:2272.

Velleman, S. G. 2020. Pectoralis major (breast) muscle extracellular matrix fibrillar collagen modifications associated with the wooden breast fibrotic myopathy in broilers. Front. Physiol. 11:461.

Vukotić, M., S. Kapor, T. Dragojević, D. Đikić, O. Mitrović Ajtić, M. Diklić, T. Subotički, E. Živković, B. Beleslin Čokić, A. Vojvodić, J. F. Santibáñez, M. Gotić, and V. P. Čokić. 2022. Inhibition of proinflammatory signaling impairs fibrosis of bone marrow mesenchymal stromal cells in myeloproliferative neoplasms. Exp. Mol. Med. 54:273–284.

Widjaja, A. A., S. Chothani, S. Viswanathan, J. W. T. Goh, W. W. Lim, and S. A. Cook. 2022. IL11 stimulates IL33 expression and proinflammatory fibroblast activation across tissues. Int. J. Mol. Sci. 23:8900.

Xing, T., D. Luo, X. Zhao, X. L. Xu, J. l. Li, L. Zhang, and F. Gao. 2021a. Enhanced cytokine expression and upregulation of inflammatory signaling pathways in broiler chickens affected by wooden breast myopathy. J. Sci. Food Agric. 101:279–286.

Xing, T., X. Pan, L. Zhang, and F. Gao. 2021b. Hepatic oxidative stress, apoptosis, and inflammation in broiler chickens with wooden breast myopathy. Front. Physiol. 12:659777.

Xing, T., X. Zhao, L. Zhang, J. L. Li, G. H. Zhou, X. L. Xu, and F. Gao. 2020. Characteristics and incidence of broiler chicken wooden breast meat under commercial conditions in China. Poult. Sci. 99:620–628.

Xing, T., Z. R. Zhao, X. Zhao, X. L. Xu, L. Zhang, and F. Gao. 2021c. Enhanced transforming growth factor-beta signaling and fibrosis in the pectoralis major muscle of broiler chickens affected by wooden breast myopathy. Poult. Sci. 100:100804.

Xu, T., M. M. Ni, L. Xing, X. F. Li, X. M. Meng, C. Huang, and J. Li. 2016. NLRC5 regulates TGF-beta1-induced proliferation and activation of hepatic stellate cells during hepatic fibrosis. Int. J. Biochem. Cell. Biol. 70:92–104.

Yang, Y., S. C. Kim, T. Yu, Y. S. Yi, M. H. Rhee, G. H. Sung, B. C. Yoo, and J. Y. Cho. 2014. Functional roles of p38 mitogen-activated protein kinase in macrophage-mediated inflammatory responses. Mediators Inflamm. 2014:352371.

Yu, G., L. G. Wang, Y. Han, and Q. Y. He. 2012. clusterProfiler: an R package for comparing biological themes among gene clusters. OMICS 16:284–287.

Zhang, N., M. H. Ahsan, L. Zhu, L. C. Sambucetti, A. F. Purchio, and D. B. West. 2005. Regulation of IkappaBalpha expression involves both NF-kappaB and the MAP kinase signaling pathways. J. Inflamm. (Lond.) 2:10.

Zhang, T., T. Wang, Q. Niu, L. Xu, Y. Chen, X. Gao, H. Gao, L. Zhang, G. E. Liu, J. Li, and L. Xu. 2022. Transcriptional atlas analysis from multiple tissues reveals the expression specificity patterns in beef cattle. BMC Biol. 20:79.